Bridging the Gap Between the Babinet Principle and the Physical Optics Approximation: Scalar Problem

Gildas Kubické, Yacine Ait Yahia, Christophe Bourlier, *Member, IEEE*, Nicolas Pinel, *Associate Member, IEEE*, and Philippe Pouliguen

Abstract—For a two-dimensional (2-D) problem, this paper shows that the Babinet Principle (BP) can be derived from the physical optics (PO) approximation. Indeed, following the same idea as Ufimtsev, from the PO approximation and in far-field zone, the field scattered by an object can be split up into a field that mainly contributes around the specular direction (illuminated zone) and a field that mainly contributes around the forward direction (shadowed zone), which is strongly related to the scattered field obtained from the BP. The only difference relies on the integration surface. We also show mathematically that the involved integral does not depend on the shape of the object, which then corresponds to the BP. Simulations are provided to illustrate the link between the BP and PO.

Index Terms—Babinet principle, forward scattering, physical optics, shadow radiation.

I. INTRODUCTION

THE ELECTROMAGNETIC wave scattering from a target in the forward scattering (FS) region (when the target lies on the transmitter–receiver baseline) [1] is a very interesting phenomenon and was first reported by Mie in 1908, when he discovered that the forward-scattered energy produced by a sphere was larger than the backscattered energy [2] in high-frequency domain. This configuration, which corresponds to a bistatic angle (θ_s-θ_i) near 180° (see Fig. 1), is a potential solution to detect stealth targets. Indeed, in high-frequency domain, the forward-scattering radar cross section (RCS) is mainly determined by the silhouette of the target seen by the transmitter and is almost unaffected by stealth absorbing coatings or shapings. This phenomenon can be physically explained by the fact that the scattered field in the forward direction represents the perturbation to the incident wave as a blocking effect that creates a shadowed zone behind the target. In this region, while the total field vanishes, the scattered field tends to the incident field (in amplitude) but in opposite phase. A simple explanation can be given using the Babinet principle (BP) [1], which states that
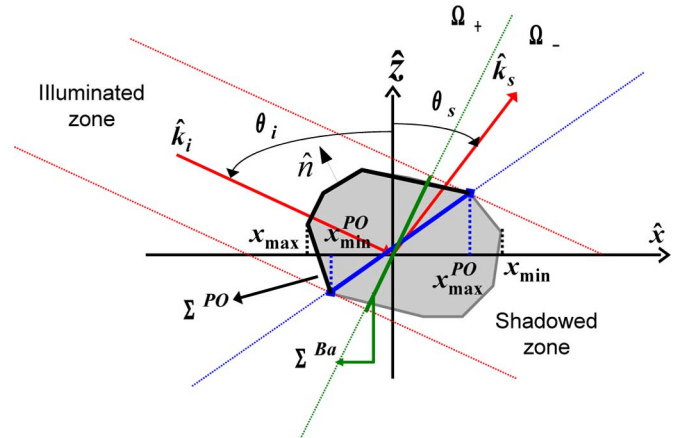
Fig. 1. Geometry of the problem: The target is illuminated by an incident field, and a shadowed zone is produced behind the object. The projection of the object illuminated surface Σ_{PO} onto the plane orthogonal to the incident direction and centered on the phase origin is Σ_{Ba}. The plane orthogonal to the incident direction splits the space into two subdomains: the illuminated zone Ω_+ and the shadowed zone Ω_-.

the diffraction pattern (in forward direction) of an opaque body is identical to that of a hole (in a perfectly conducting screen) having the same shape as its silhouette.

Nevertheless, the physical optics (PO) approximation is sometimes used instead of the BP [2]–[4] and provides good results near the forward direction. Ufimtsev [5]–[8] studied the shadow radiation and demonstrated that the PO approximation can be split up into two components [5], [8]: one that mainly contributes in the backward direction and thus corresponds to a reflected component, and the other one that mainly contributes in the forward direction and thus corresponds to a shadowed component. In this paper, the link between the BP and the PO approximations is provided. First, a theoretical study is presented, and then numerical results compare theses two asymptotic approaches. The time convention $e^{-j\omega t}$ is omitted throughout the paper.

II. THEORETICAL STUDY

A. PO Approximation

Induced currents on the object surface can be estimated by using the PO approximation. For a 3-D (vectorial) problem, PO currents are given by the well-known expressions

$$\begin{cases} \boldsymbol{J}(\boldsymbol{r}) = \hat{\boldsymbol{n}}(\boldsymbol{r}) \wedge [\boldsymbol{H_i}(\boldsymbol{r}) + \bar{\boldsymbol{R}}_{\boldsymbol{H}}\boldsymbol{H_i}(\boldsymbol{r})] \\ \boldsymbol{M}(\boldsymbol{r}) = -\hat{\boldsymbol{n}}(\boldsymbol{r}) \wedge [\boldsymbol{E_i}(\boldsymbol{r}) + \bar{\boldsymbol{R}}_{\boldsymbol{E}}\boldsymbol{E_i}(\boldsymbol{r})] \end{cases} \quad \boldsymbol{r} \in \Sigma_{\mathrm{PO}} \quad (1)$$

where $\hat{n}$ is the unitary normal vector to the surface, $\boldsymbol{r} = (x, y, z(x, y))$ is a position vector on the surface, $\boldsymbol{J}$ and $\boldsymbol{M}$ are the electric and magnetic currents, respectively, and $\bar{R}_H$ and $\bar{R}_E$ are the reflection matrices given from the Fresnel reflection coefficients

$$\bar{R}_H = \begin{bmatrix} \mathcal{R}_\perp & 0 \\ 0 & \mathcal{R}_\| \end{bmatrix} \quad \bar{R}_E = \begin{bmatrix} \mathcal{R}_\| & 0 \\ 0 & \mathcal{R}_\perp \end{bmatrix}. \tag{2}$$

By assuming that the scene is invariant according $\hat{\boldsymbol{y}}$-direction, then the problem becomes scalar. For the TE polarization (electric field in the $\hat{\boldsymbol{y}}$-direction), the unknown ψ is the transverse component of the electric field ($\boldsymbol{E} = \psi \hat{\boldsymbol{y}}$). Then, one can show that

$$\boldsymbol{J}(\boldsymbol{r}) = \hat{\boldsymbol{n}} \wedge \boldsymbol{H} = \frac{\partial \psi(\boldsymbol{r})}{\partial n} \left(-\frac{\hat{\boldsymbol{y}}}{j\omega\mu} \right) \tag{3}$$

$$\boldsymbol{M}(\boldsymbol{r}) = -\hat{\boldsymbol{n}} \wedge \boldsymbol{E} = \psi(-\hat{\boldsymbol{n}} \wedge \hat{\boldsymbol{y}}). \tag{4}$$

This leads to an equivalence between 3-D and 2-D problems for the TE polarization

$$\boldsymbol{J}(\boldsymbol{r}) \longleftrightarrow \frac{\partial \psi(\boldsymbol{r})}{\partial n} \quad \boldsymbol{M}(\boldsymbol{r}) \longleftrightarrow \psi. \tag{5}$$

From a similar way for the TM polarization (magnetic field in the $\hat{\boldsymbol{y}}$-direction), one can define the equivalence between 3-D and 2-D problems

$$\boldsymbol{J}(\boldsymbol{r}) \longleftrightarrow \psi(\boldsymbol{r}) \quad \boldsymbol{M}(\boldsymbol{r}) \longleftrightarrow \frac{\partial \psi(\boldsymbol{r})}{\partial n}. \tag{6}$$

For a 2-D (scalar) problem, assuming an incident plane wave on the target, PO currents are given by

$$\begin{cases} \psi(\boldsymbol{r}) = [1 + \mathcal{R}(\theta)]\psi_i \\ \frac{\partial \psi(\boldsymbol{r})}{\partial n} = j\boldsymbol{k}_i \cdot \hat{\boldsymbol{n}}[1 - \mathcal{R}(\theta)]\psi_i \end{cases} \quad \boldsymbol{r} \in \Sigma_{\text{PO}} \tag{7}$$

where $\boldsymbol{r} = (x, z(x)) = x\hat{\boldsymbol{x}} + z(x)\hat{\boldsymbol{z}}$ is a vector on the surface, $\psi(\boldsymbol{r})$ the total field on the surface, and $(\partial\psi(\boldsymbol{r}))/(\partial n) = \nabla\psi \cdot \hat{\boldsymbol{n}}$ its normal derivative. The latter two quantities are the unknowns of the problem. Moreover, $\hat{\boldsymbol{n}} = v(x)(-\gamma(x)\hat{\boldsymbol{x}} + \hat{\boldsymbol{z}})/(\sqrt{1 + \gamma^2(x)})$ is the unitary normal vector to the surface, in which $v(x)$ defines the orientation of the normal vector ($v(x) = \text{sign}(\hat{\boldsymbol{n}} \cdot \hat{\boldsymbol{z}})$) and $\gamma(x) = (dz)/(dx)$ is the surface slope. $\boldsymbol{k}_i$ is the incident wave vector, $\mathcal{R}$ is the Fresnel reflection coefficient, which depends on $\boldsymbol{r}$; for a perfectly conducting object, $\mathcal{R}(\theta) = \pm 1$ for TM and TE polarizations, respectively. Lastly, Σ_{PO} is the target illuminated surface (see Fig. 1). Contrary to the Babinet induced currents (see below), PO currents have physical meaning and tend to the tangential fields measured at the object surface. The radiation of these currents is computed from the Huygens principle [10], $\forall \boldsymbol{r}'$

$$\psi_s(\boldsymbol{r}') = \int_\Sigma \left[\psi(\boldsymbol{r}) \frac{\partial g(\boldsymbol{r}, \boldsymbol{r}')}{\partial n} - g(\boldsymbol{r}, \boldsymbol{r}') \frac{\partial \psi(\boldsymbol{r})}{\partial n} \right] d\Sigma, \tag{8}$$

where $g(\boldsymbol{r}, \boldsymbol{r}')$ is the 2-D (scalar) Green function, with $\boldsymbol{r}' = (x', z') = x'\hat{\boldsymbol{x}} + z'\hat{\boldsymbol{z}}$ the observation vector. Thus, assuming the target in far field from the receiver, $\forall \boldsymbol{r}'$, substituting (7) into (8), one has

$$\psi_{s,\text{PO}}(\boldsymbol{r}')$$
$$= g_\infty \int_{\Sigma_{\text{PO}}} [(\hat{\boldsymbol{n}} \cdot \boldsymbol{k}_s)(1 + \mathcal{R}) + (\hat{\boldsymbol{n}} \cdot \boldsymbol{k}_i)(1 - \mathcal{R})]$$
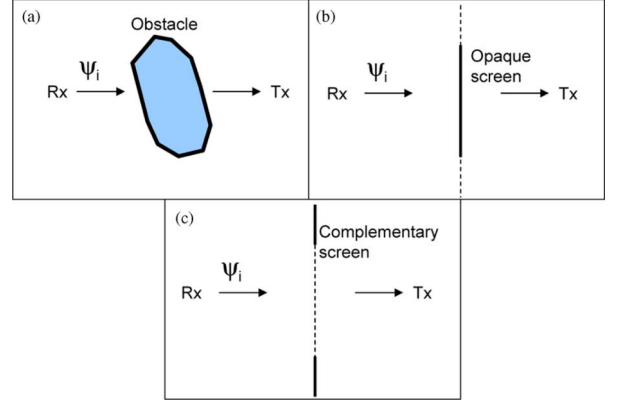

Fig. 2. Babinet principle. (a) Forward scattering from an arbitrary obstacle. (b) Forward scattering from the associated opaque screen. (c) Diffraction from the complementary screen = a hole in the infinite plane.

$$\times e^{-j(\boldsymbol{k}_s - \boldsymbol{k}_i) \cdot \boldsymbol{r}} d\Sigma$$
$$= g_\infty \underbrace{\int_{\Sigma_{\text{PO}}} \mathcal{R}\hat{\boldsymbol{n}} \cdot (\boldsymbol{k}_s - \boldsymbol{k}_i)e^{-j(\boldsymbol{k}_s - \boldsymbol{k}_i) \cdot \boldsymbol{r}} d\Sigma}_{\psi_{s,+} = g_\infty I_+}$$
$$+ g_\infty \underbrace{\int_{\Sigma_{\text{PO}}} \hat{\boldsymbol{n}} \cdot (\boldsymbol{k}_s + \boldsymbol{k}_i)e^{-j(\boldsymbol{k}_s - \boldsymbol{k}_i) \cdot \boldsymbol{r}} d\Sigma}_{\psi_{s,-} = g_\infty I_-}, \tag{9}$$

where $g_\infty = (1/4)\sqrt{(2/(\pi k r'))}e^{j(kr' - \pi/4)}$ is related to the far-field 2-D Green function (the incident field is assumed to be unitary on the target). The last two lines of (9) correspond to the decomposition proposed by Ufimtsev [5], [8]. Ufimtsev then showed that $\psi_{s,+} = g_\infty I_+$ mainly contributes in the specular direction and thus corresponds to a "reflected" component that we call "PO reflection." Moreover, $\psi_{s,-} = g_\infty I_-$ mainly contributes in the forward direction and thus corresponds to a "shadowed" component that we call "PO forward."

B. BP

The BP is an optical principle [11] (generalized to electromagnetics [12], [13]) that states that the diffraction pattern of an opaque body is identical to that of a hole having the same shape as its silhouette (see Fig. 2). Thus, according to this principle, the FS phenomenon is independent of the shape of the object; the scattering is only due to the target area projected onto the plane orthogonal to the incident direction (see Fig. 2): the silhouette of the target. The equivalent induced currents on the aperture are only due to the presence of the incident field

$$\begin{cases} \psi(\boldsymbol{r}) = \psi_i(\boldsymbol{r}) \\ \frac{\partial \psi(\boldsymbol{r})}{\partial n} = \frac{\partial \psi_i(\boldsymbol{r})}{\partial n} \end{cases} \quad \boldsymbol{r} \in \Sigma_{\text{Ba}}. \tag{10}$$

As depicted in Fig. 1, the plane orthogonal to the incident direction splits the space into two subdomains: the illuminated zone Ω_+ and the shadowed zone Ω_-. Σ_{Ba} is the target area projected onto the plane orthogonal to the incident direction and centered on the phase origin, thus $\hat{\boldsymbol{n}} = \hat{\boldsymbol{z}}$ in the case of normal incidence ($\hat{\boldsymbol{n}}$ being the normal of Σ_{Ba} here). It must be noted that the normal incidence case can be considered with no assumption. Indeed, by a rotation of the problem, one can make variable changes to always consider a local system of coordinates in which the incident wave vector is in the sense of negative z.

Moving the emitter with a fixed target is equivalent to rotating the target with a fixed emitter.

In the far field (the receiver is in far field from the screen), the substitution of (10) into (8) leads, for any polarization and $\forall \boldsymbol{r}' \in \Omega_-$, to

$$
\begin{aligned}
\psi_{s,\mathrm{Ba}}(\boldsymbol{r}') &= g_\infty I_{\mathrm{Ba}} \\
&= g_\infty \int_{\Sigma_{\mathrm{Ba}}} \hat{\boldsymbol{n}} \cdot (\boldsymbol{k}_s + \boldsymbol{k}_i) e^{-j(\boldsymbol{k}_s - \boldsymbol{k}_i)\cdot\boldsymbol{r}}\, d\Sigma. \quad (11)
\end{aligned}
$$

Comparing (11) to (9), if $I_{\mathrm{Ba}} = I_-$, we can write

$$
\psi_{s,\mathrm{PO}}(\boldsymbol{r}') = g_\infty I_{\mathrm{Ba}} + g_\infty I_+ \quad (12)
$$

so

$$
\begin{aligned}
&\int_{\Sigma_{\mathrm{Ba}}} \hat{\boldsymbol{n}} \cdot (\boldsymbol{k}_s + \boldsymbol{k}_i) e^{-j(\boldsymbol{k}_s - \boldsymbol{k}_i)\cdot\boldsymbol{r}}\, d\Sigma \\
&= \int_{\Sigma_{\mathrm{PO}}} \hat{\boldsymbol{n}} \cdot (\boldsymbol{k}_s + \boldsymbol{k}_i) e^{-j(\boldsymbol{k}_s - \boldsymbol{k}_i)\cdot\boldsymbol{r}}\, d\Sigma. \quad (13)
\end{aligned}
$$

In other words, equality (12) is satisfied if the integral is independent of the surface integration Σ. The proof of this statement is given next.

C. Proof: "Shadowed" Component

By setting

$$
\begin{cases}
a_1 = (\boldsymbol{k}_s + \boldsymbol{k}_i) \cdot \hat{\boldsymbol{x}} = k(\sin\theta_s + \sin\theta_i) \\
b_1 = (\boldsymbol{k}_s + \boldsymbol{k}_i) \cdot \hat{\boldsymbol{z}} = k(\cos\theta_s - \cos\theta_i) \\
a_2 = (\boldsymbol{k}_s - \boldsymbol{k}_i) \cdot \hat{\boldsymbol{x}} = k(\sin\theta_s - \sin\theta_i) \\
b_2 = (\boldsymbol{k}_s - \boldsymbol{k}_i) \cdot \hat{\boldsymbol{z}} = k(\cos\theta_s + \cos\theta_i)
\end{cases} \quad (14)
$$

and since $\hat{\boldsymbol{n}} = \hat{\boldsymbol{z}}$ (normal incidence), $d\Sigma = dx$, and $\forall \boldsymbol{r} \in \Sigma_{\mathrm{Ba}}$, I_{Ba} in (13) becomes

$$
\begin{aligned}
I_{\mathrm{Ba}} &= \frac{jb_1}{a_2} \left[e^{-ja_2 x - jb_2 z(x)} \right]_{x_{\min}^{\mathrm{Ba}}}^{x_{\max}^{\mathrm{Ba}}} \\
&= b_1 L\, \mathrm{sinc}\left(\frac{a_2 L}{2} \right) \quad (15)
\end{aligned}
$$

with L the length of the screen.

Since $\hat{\boldsymbol{n}} = (-\gamma(x)\hat{\boldsymbol{x}} + \hat{\boldsymbol{z}})/(\sqrt{1 + \gamma^2(x)})$ $\forall \boldsymbol{r} \in \Sigma_{\mathrm{PO}}$ (the normal vector on Σ_{PO} is assumed to be oriented in the sense of positive $\hat{\boldsymbol{z}}$: $v(x) = +1$), $d\Sigma = \sqrt{1 + \gamma^2(x)}\,dx$, and $\int u'(x) e^{-ju(x)} dx = je^{-ju(x)}$, I_- in (13) becomes

$$
\begin{aligned}
I_- &= \int_{x_{\min}^{\mathrm{PO}}}^{x_{\max}^{\mathrm{PO}}} [-a_1 \gamma(x) + b_1] e^{-ja_2 x - jb_2 z(x)}\, dx \\
&= \frac{a_1}{b_2} \int_{x_{\min}^{\mathrm{PO}}}^{x_{\max}^{\mathrm{PO}}} \left[-\gamma(x) b_2 - a_2 + \frac{b_1 b_2}{a_1} + a_2 \right] \\
&\quad \times e^{-ja_2 x - jb_2 z(x)}\, dx \\
&= \frac{a_1}{jb_2} \left[e^{-ja_2 x - jb_2 z(x)} \right]_{x_{\min}^{\mathrm{PO}}}^{x_{\max}^{\mathrm{PO}}} \\
&\quad + \left(\frac{b_1 b_2}{a_1} + a_2 \right) \int_{x_{\min}^{\mathrm{PO}}}^{x_{\max}^{\mathrm{PO}}} e^{-ja_2 x - jb_2 z(x)}\, dx \quad (16)
\end{aligned}
$$

where $x_{\min}^{\mathrm{PO}}$ and $x_{\max}^{\mathrm{PO}}$ are the lower and upper values of the abscissa of the illuminated surface Σ_{PO}, respectively.

Since $a_1 a_2 + b_1 b_2 = 0$ $\forall(\theta_i, \theta_s)$, (16) becomes

$$
\begin{aligned}
I_- &= \frac{a_1}{jb_2} \left[e^{-ja_2 x - jb_2 z(x)} \right]_{x_{\min}^{\mathrm{PO}}}^{x_{\max}^{\mathrm{PO}}} \\
&= \frac{2Aa_1}{b_2} e^{jB}\, \mathrm{sinc}(A) \quad (17)
\end{aligned}
$$

where

$$
A = -\frac{a_2 x_m + b_2 z_m}{2} \quad B = -\frac{a_2 x_p + b_2 z_p}{2} \quad (18)
$$

and

$$
\begin{cases}
x_m = x_{\max}^{\mathrm{PO}} - x_{\min}^{\mathrm{PO}} & z_m = z\left(x_{\max}^{\mathrm{PO}} \right) - z\left(x_{\min}^{\mathrm{PO}} \right) \\
x_p = x_{\max}^{\mathrm{PO}} + x_{\min}^{\mathrm{PO}} & z_p = z\left(x_{\max}^{\mathrm{PO}} \right) + z\left(x_{\min}^{\mathrm{PO}} \right)
\end{cases}. \quad (19)
$$

It must be noted that $x_p = 0$ and $x_m = L$ for an object of length L (along $\hat{\boldsymbol{x}}$-direction) centered on the phase origin. Then, the PO forward component is expressed from a sinc function and does not depend on the object shape. This is consistent with the "Shadow Contour Theorem" [5], [8], which states that, *"The shadow radiation does not depend on the whole shape of the scattering object, and is completely determined only by the size and the geometry of the shadow contour."*

Thus, equality between the PO forward component and BP in (13) holds if equality is obtained between (15) and (17). This holds for either of the following:

- $B = 0$ and $z_m = 0$: the two limit points of Σ_{PO} are the same as those of the complementary Babinet screen Σ_{Ba}, i.e., $(x_{\min}^{\mathrm{PO}}, z(x_{\min}^{\mathrm{PO}})) = (x_{\min}^{\mathrm{Ba}}, 0)$ and $(x_{\max}^{\mathrm{PO}}, z(x_{\max}^{\mathrm{PO}})) = (x_{\max}^{\mathrm{Ba}}, 0)$;

or

- $b_2 = 0$ implying $\theta_s = \pi - \theta_i$, which corresponds to the FS direction, for which $\boldsymbol{k}_i$ and $\boldsymbol{k}_s$ are collinear.

It must be noted that, even with $x_p = 0$, if $z_p \neq 0$, then $B \neq 0$ (except for $\theta_s = \pi - \theta_i$: the FS direction) and $(x_{\min}^{\mathrm{PO}}, z(x_{\min}^{\mathrm{PO}})) = (x_{\min}^{\mathrm{Ba}}, z_p)$ and $(x_{\max}^{\mathrm{PO}}, z(x_{\max}^{\mathrm{PO}})) = (x_{\max}^{\mathrm{Ba}}, z_p)$: There is only a shift of the PO surface in $\hat{\boldsymbol{z}}$ direction, which implies a constant phase shift (described by the term e^{jB}) of the scattered field. Thus, it must be highlighted that even for $z_p \neq 0$, equality between the two approaches remains in terms of RCS.

D. "Reflected" Component

Using the same way for the "reflected" component (I_+), it can be shown from (9) and for a perfectly conducting ($\mathcal{R} = \pm 1$) object that

$$
I_+ = \pm \int_{x_{\min}^{\mathrm{PO}}}^{x_{\max}^{\mathrm{PO}}} [-a_2 \gamma(x) + b_2] e^{-ja_2 x - jb_2 z(x)}\, dx \quad (20)
$$

and for $a_2 \neq 0$

$$I_+ = \pm \frac{a_2}{jb_2} \left[e^{-ja_2 x - jb_2 z(x)} \right]_{x_{\min}^{\mathrm{PO}}}^{x_{\max}^{\mathrm{PO}}}$$
$$\pm \left(\frac{b_2^2}{a_2} + a_2 \right) \int_{x_{\min}^{\mathrm{PO}}}^{x_{\max}^{\mathrm{PO}}} e^{-ja_2 x - jb_2 z(x)} \, dx$$
$$= \pm \frac{2Aa_2}{b_2} e^{jB} \mathrm{sinc}(A)$$
$$\pm \left(\frac{b_2^2}{a_2} + a_2 \right) \int_{x_{\min}^{\mathrm{PO}}}^{x_{\max}^{\mathrm{PO}}} e^{-ja_2 x - jb_2 z(x)} \, dx \qquad (21)$$

where

$$b_2^2 + a_2^2 = 4k^2 \cos^2 \left(\frac{\theta_s + \theta_i}{2} \right)$$
$$\frac{a_2}{b_2} = \tan \left(\frac{\theta_s - \theta_i}{2} \right). \qquad (22)$$

Unlike the field "shadowed component," (21) shows that the field in the illuminated zone depends on the surface profile *a priori* because $b_2^2 + a_2^2 \neq 0$ in the illuminated zone.

E. Discussion

In the reflected direction defined by $\theta_s = \theta_i$ (corresponding to the specular direction for an horizontal plate), from (14), one has

$$\begin{cases} a_1 = 2k \sin \theta_i & b_2 = 2k \cos \theta_i \\ a_2 = 0 & b_1 = 0 \\ A = -kz_m \cos \theta_i & B = -kz_p \cos \theta_i \\ \frac{2Aa_1}{b_2} = -2kz_m \sin \theta_i & \frac{2Aa_2}{b_2} = 0 \\ b_2^2 + a_2^2 = 4k^2 \cos^2 \theta_i. \end{cases} \qquad (23)$$

Equations (17) and (20) then become

$$\begin{cases} I_- = -2kz_m \sin \theta_i e^{-jkz_p \cos \theta_i} \mathrm{sinc}(kz_m \cos \theta_i) \\ I_+ = \pm 2k \cos \theta_i \int_{x_{\min}^{\mathrm{PO}}}^{x_{\max}^{\mathrm{PO}}} e^{-jb_2 z(x)} \, dx. \end{cases} \qquad (24)$$

Since we consider normal incidence ($\theta_i = 0$), the above equation clearly shows that the component I_- vanishes in the specular direction. Moreover, if $z_m = 0$, then $I_- = 0 \; \forall \theta_i$. On the contrary, the component I_+ strongly contributes in the specular direction.

In the forward direction defined as $\theta_s = \pi - \theta_i$, from (14), one has

$$\begin{cases} a_1 = 2k \sin \theta_i & b_2 = 0 \\ a_2 = 0 & b_1 = -2k \cos \theta_i \\ A = 0 & B = 0 \\ \frac{2Aa_1}{b_2} = -2k(x_m \cos \theta_i + z_m \sin \theta_i) & \frac{2Aa_2}{b_2} = 0 \\ b_2^2 + a_2^2 = 0. \end{cases} \qquad (25)$$

Equations (17) and (20) then become

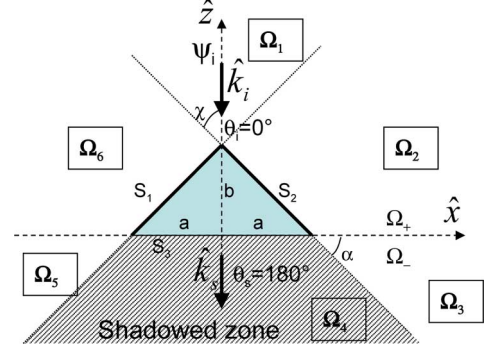$$\begin{cases} I_- = -2k(x_m \cos \theta_i + z_m \sin \theta_i) \\ I_+ = 0. \end{cases} \qquad (26)$$

Fig. 3. Forward scattering from a triangularly shaped target. The two sub-domains Ω_+ ($z > 0$) and Ω_- ($z < 0$) can be decomposed into $\Omega_+ = \Omega_1 \cup \Omega_2 \cup \Omega_6$ and $\Omega_- = \Omega_3 \cup \Omega_4 \cup \Omega_5$.

This equation clearly shows that the component I_- strongly contributes in the forward direction and depends on x_m, which is related to the length of the object. On the contrary, the component I_+ vanishes in the forward direction.

As the main conclusion of Section II, the BP is a good approximation of the PO near the FS direction and $\psi_{s,\mathrm{Ba}}(\boldsymbol{r}') \to \psi_{s,\mathrm{PO}}(\boldsymbol{r}')$ when $\psi_{s,+} \to 0$ for $\theta_s \to \pi - \theta_i$. The BP is then a particular case of the PO approach.

III. NUMERICAL RESULTS

A. Combining PO and BP for a Triangular Target

Let us consider the scene given in Fig. 3, in which a triangularly shaped target is illuminated by an incident plane wave.

The lengths of the three elementary planar surfaces S_1, S_2, and S_3 are $L_1 = L_2 = \sqrt{a^2 + b^2}$ and $L_3 = 2a$, respectively. As can be seen, $\Sigma_{\mathrm{PO}} = S_1 \cup S_2$ and $\Sigma_{\mathrm{Ba}} = S_3$. Edge diffraction is neglected because the work is focused here on the FS phenomenon. Since $\Sigma_{\mathrm{PO}} = S_1 \cup S_2$, under the PO approximation, ψ_s can be written as

$$\psi_{s,\mathrm{PO}}(\boldsymbol{r}') = \psi_{s,1+} + \psi_{s,1-} + \psi_{s,2+} + \psi_{s,2-} \qquad (27)$$

in which, for $p = \{1; 2\}$

$$\psi_{s,p+} = g_\infty \int_{S_p} \mathcal{R} \hat{\boldsymbol{n}} \cdot (\boldsymbol{k}_s - \boldsymbol{k}_i) e^{-j(\boldsymbol{k}_s - \boldsymbol{k}_i) \cdot \boldsymbol{r}} \, d\Sigma$$
$$\psi_{s,p-} = g_\infty \int_{S_p} \hat{\boldsymbol{n}} \cdot (\boldsymbol{k}_s + \boldsymbol{k}_i) e^{-j(\boldsymbol{k}_s - \boldsymbol{k}_i) \cdot \boldsymbol{r}} d\Sigma \qquad (28)$$

which simplifies as

$$\psi_{s,p+}$$
$$= \mathcal{R} g_\infty a [b_2 - \gamma_p a_2] \mathrm{sinc} \left((a_2 + b_2 \gamma_p) \frac{a}{2} \right) e^{jc_p a_2 \frac{a}{2} - jb_2 \frac{b}{2}}$$
$$\psi_{s,p-}$$
$$= g_\infty a [b_1 - \gamma_p a_1] \mathrm{sinc} \left((a_2 + b_2 \gamma_p) \frac{a}{2} \right) e^{jc_p a_2 \frac{a}{2} - jb_2 \frac{b}{2}}$$
$$\qquad (29)$$

in which $\gamma_p = c_p(b/a)$, and $c_p = \pm 1$ for $p = 1$ or 2, respectively.

The BP states that for a receiver in far field located inside $\Omega_- = \Omega_3 \cup \Omega_4 \cup \Omega_5$, the scattered field is given from (15), with $L = L_3$. This result is relevant for the subdomain Ω_4 for which the receiver is in the shadowed zone of the target, but results can be wrong in subdomains Ω_3 and Ω_5 in which the receiver is not in the shadowed zone of S_2 and S_1, respectively. That is to say, S_1 contributes in reflection in Ω_5. Indeed and more generally, it can be observed that the "shadowed" zone of S_1 is $\Omega_2 \cup \Omega_3 \cup \Omega_4$, whereas the "shadowed" zone of S_2 is $\Omega_4 \cup \Omega_5 \cup \Omega_6$. Thus, a means to obtain the scattered field is to compute the PO for the reflection from S_1 and the BP for forward scattering from S_2 [14]. Then, for each subdomain, one obtains

$$
\psi_{s,\mathrm{Ba+PO}}(\boldsymbol{r}')
$$
$$
= \begin{cases}
\psi_{s,1,\mathrm{PO}}(\boldsymbol{r}') + \psi_{s,2,\mathrm{PO}}(\boldsymbol{r}') & \forall \boldsymbol{r}' \in \Omega_1 \\
\psi_{s,1,\mathrm{Ba}}(\boldsymbol{r}') + \psi_{s,2,\mathrm{PO}}(\boldsymbol{r}') & \forall \boldsymbol{r}' \in \Omega_2 \cup \Omega_3 \\
\psi_{s,1,\mathrm{Ba}}(\boldsymbol{r}') + \psi_{s,2,\mathrm{Ba}}(\boldsymbol{r}') & \forall \boldsymbol{r}' \in \Omega_4 \\
\psi_{s,1,\mathrm{PO}}(\boldsymbol{r}') + \psi_{s,2,\mathrm{Ba}}(\boldsymbol{r}') & \forall \boldsymbol{r}' \in \Omega_5 \cup \Omega_6
\end{cases} \quad (30)
$$

in which, for $p = \{1; 2\}$, $\psi_{s,p,\mathrm{PO}}(\boldsymbol{r}') = g_\infty(\psi_{s,p+} + \psi_{s,1-})$ and $\psi_{s,p,\mathrm{Ba}}(\boldsymbol{r}')$ is obtained by using the Babinet induced currents on the surface S_p. This corresponds to (11), but on the surface S_p. It can be noticed that the integrand in (11) is exactly the same as the one in the term $\psi_{s,-}$ of (9), which leads to $\psi_{s,p,\mathrm{Ba}}(\boldsymbol{r}') = \psi_{s,p-}$. Then, (30) can be written in terms of $\psi_{s,p,\pm}$ as

$$
\psi_{s,\mathrm{Ba+PO}}(\boldsymbol{r}')
$$
$$
= \begin{cases}
\psi_{s,1+} + \psi_{s,1-} + \psi_{s,2+} + \psi_{s,2-} & \forall \boldsymbol{r}' \in \Omega_1 \\
\psi_{s,1-} + \psi_{s,2+} + \psi_{s,2-} & \forall \boldsymbol{r}' \in \Omega_2 \cup \Omega_3 \\
\psi_{s,1-} + \psi_{s,2-} & \forall \boldsymbol{r}' \in \Omega_4 \\
\psi_{s,1+} + \psi_{s,1-} + \psi_{s,2-} & \forall \boldsymbol{r}' \in \Omega_5 \cup \Omega_6.
\end{cases} \quad (31)
$$

Using PO combined with BP on each elementary surface implies that the $\psi_{s,p+}$ component is neglected in the shadowed zone of the surface S_p. According to PO, $\psi_{s,p+}$ is much lower than $\psi_{s,p-}$ in the FS direction of S_p, but this can induce slight discontinuities in the RCS at the subdomain frontiers. Thus, PO + BP can be seen as an approximation of PO.

B. RCS of the Triangular Target

The RCS is defined in the 2-D case as

$$
\sigma = \lim_{r' \to \infty} 2\pi r' \frac{|\psi_s(\boldsymbol{r}')|^2}{|\psi_{i0}|^2}. \quad (32)
$$

Thus, the RCS computed from the PO approach is given from (32), in which $\psi_s(\boldsymbol{r}') = \psi_{s,\mathrm{PO}}(\boldsymbol{r}')$ given from (27) and (29). The RCS for the PO combined with the BP is given from (32), in which $\psi_s(\boldsymbol{r}') = \psi_{s,\mathrm{Ba+PO}}(\boldsymbol{r}')$ is given from (29) and (31).

C. First Case: $a = 5\lambda$, $b = 3\lambda$, $\theta_i = 0°$, and TE Polarization

The RCS of these two asymptotic approaches are compared to the RCS computed from a benchmark method: the well-known method of moments (MoM). The comparison is depicted in Fig. 4 versus the scattering angle θ_s for $\theta_i = 0°$ and for TE polarization. The triangularly shaped target (see Fig. 3) is defined from $a = 5\lambda$, $b = 3\lambda$, which implies $\alpha = \chi = 31°$.

As can be seen, results from the two asymptotic approaches agree well with that of the benchmark method, and in particular around the specular direction of surface S_2 ($\theta_s = 62°$)
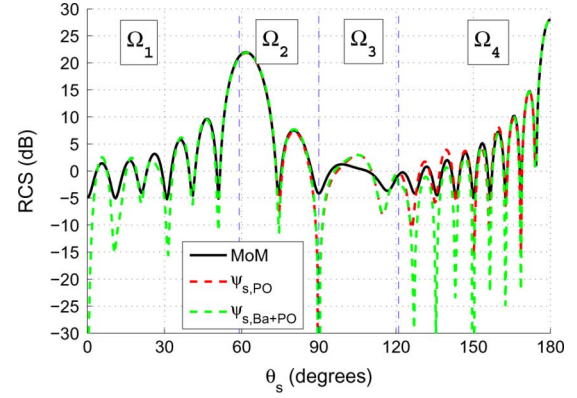

Fig. 4. RCS of the triangularly shaped target of Fig. 3 with $a = 5\lambda$, $b = 3\lambda$, for $\theta_i = 0°$ and for TE polarization, computed from the MoM, the PO, and the PO combined with the BP.
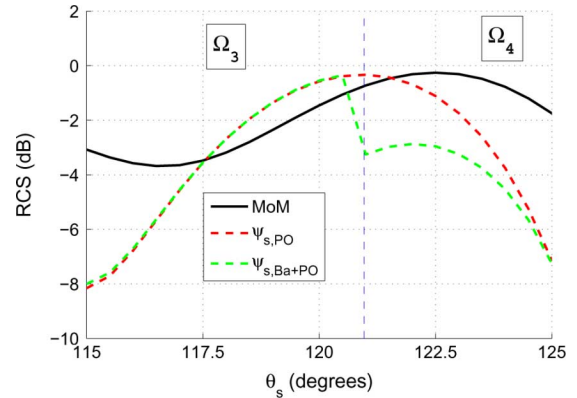

Fig. 5. Enlarged detail of Fig. 4 around the frontier between Ω_3 and Ω_4.

and around the FS direction ($\theta_s = 180°$). Slight differences between the classical PO and the PO combined with the BP can be observed for $\theta_s \in [120°; 150°]$. Indeed, $\psi_{s,1+}$ is set to zero in Ω_3, and both $\psi_{s,1+}$ and $\psi_{s,2+}$ are set to zero in Ω_4 for the computation of $\psi_{s,\mathrm{Ba+PO}}(\boldsymbol{r}')$, and as the observation angle increases, these two contributions decrease in $\psi_{s,\mathrm{PO}}(\boldsymbol{r}')$. Moreover, a slight discontinuity in the RCS computed from $\psi_{s,\mathrm{Ba+PO}}(\boldsymbol{r}')$ can be observed at the frontier between Ω_3 and Ω_4 for $\theta_s = 121°$ (an enlarged detail is depicted in Fig. 5). Indeed, from this angle, $\psi_{s,2+}$ is set to zero in PO combined with BP. This discontinuity does not appear with classical PO method.

Fig. 6 compares the RCS of $\psi_{s,\mathrm{PO}}(\boldsymbol{r}')$ and the RCS of its two components: the reflected one $\psi_{s,+}(\boldsymbol{r}')$ and the FS one $\psi_{s,-}(\boldsymbol{r}')$.

As can be seen, the scattered field from PO is mainly due to the reflected component $\psi_{s,+}(\boldsymbol{r}') \, \forall \boldsymbol{r}' \in \Omega_1 \cup \Omega_2$. In other words, the reflected component $\psi_{s,+}(\boldsymbol{r}')$ mainly contributes to the scattering process $\forall \boldsymbol{r}' \in \Omega_1 \cup \Omega_2$. For increasing θ_s from $120°$, the reflected component decreases strongly, and the FS component becomes the main contribution to the scattered field; $\psi_{s,+}(\boldsymbol{r}')$ being negligible in the shadow region Ω_4. It must be noted that this phenomenon begins to occur in subdomain Ω_3, which is in the reflected zone of S_2.

Fig. 7 compares the RCS of the FS component of PO computed from (27), in which $\psi_s(\boldsymbol{r}') = \psi_{s,-}(\boldsymbol{r}')$, and the BP given from (32), in which $\psi_s(\boldsymbol{r}') = \psi_{s,\mathrm{Ba}}(\boldsymbol{r}')$ computed from (2) and (15).
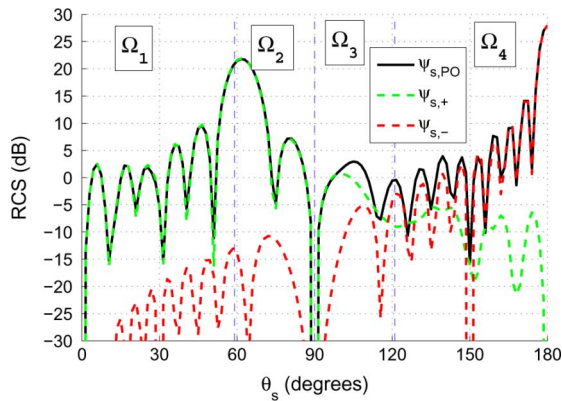
Fig. 6. Same simulation parameters as in Fig. 4, but computed from PO, PO in reflection, and PO in forward scattering.
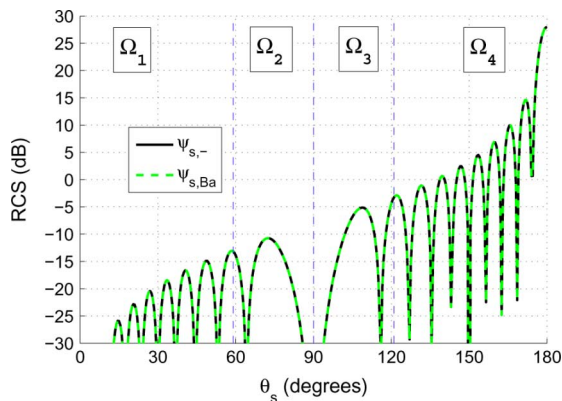

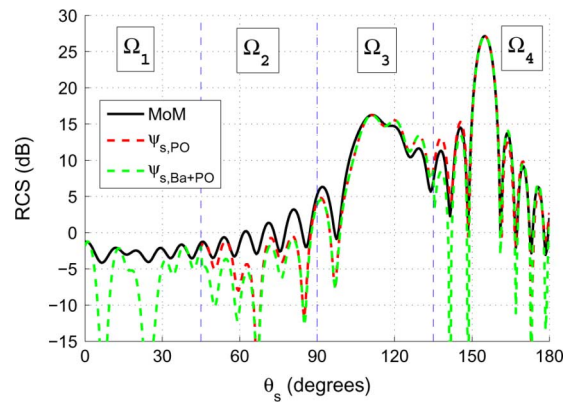Fig. 7. Same simulation parameters as in Fig. 4, but computed from PO in forward scattering and BP.

Fig. 8. RCS of the triangularly shaped target of Fig. 3 with $a = 5\lambda, b = 5\lambda$, for $\theta_i = 25°$ and for TE polarization, computed from the MoM, the PO, and the PO combined with the BP.
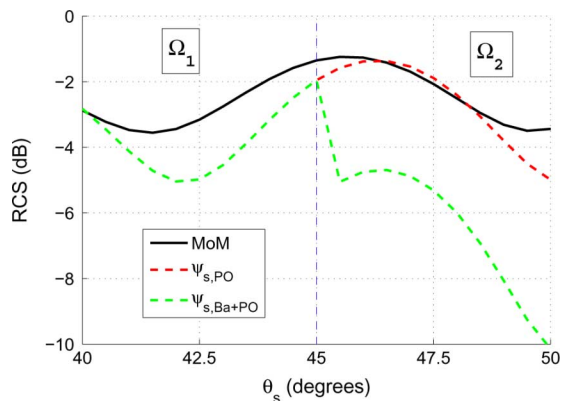

Fig. 9. Enlarged detail of Fig. 8 around the frontier between Ω_1 and Ω_2.
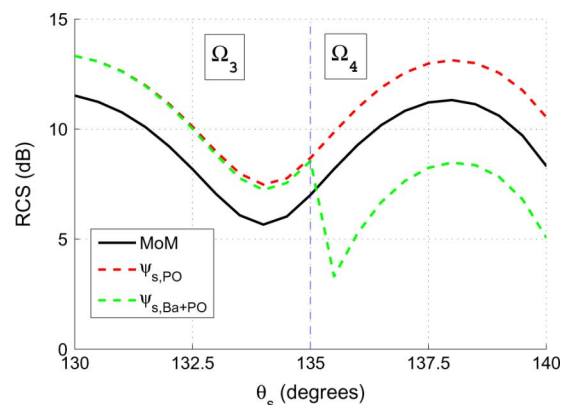

Fig. 10. Enlarged detail of Fig. 8 around the frontier between Ω_3 and Ω_4.

A perfect agreement is obtained. This illustrates the proof of equalities (12) and (13). Indeed, here $B = 0$ and $z_m = 0$ since the two limit points of Σ_{PO} are the same as those of the complementary Babinet screen Σ_{Ba} $(((x_{min}^{PO}, z(x_{min}^{PO})) = (x_{min}^{Ba}, 0))$ and $(x_{max}^{PO}, z(x_{max}^{PO})) = (x_{max}^{Ba}, 0))$. As theoretically demonstrated in Section II, in this case, the Babinet principle is included in PO approach since $\psi_{s,Ba}(\mathbf{r}') = \psi_{s,-}(\mathbf{r}')$. Interestingly, it can be noted that these results perfectly match the results obtained with other values of b: Even if the target is different, the same FS component is obtained. The shape of the illuminated surface does not play a role, which is consistent with the "Shadow Contour Theorem" [5], [8].

D. Second Case: $a = 5\lambda, b = 5\lambda, \theta_i = 25°$, and TE Polarization

The RCS of the PO and the PO combined with the BP approaches are compared to the RCS computed from the MoM in Fig. 8 versus the scattering angle θ_s for $\theta_i = 25°$ and for TE polarization. The triangularly shaped target (see Fig. 3) is now defined with $a = 5\lambda, b = 5\lambda$, and $\alpha = \chi = 45°$.

Here again, the results from the two asymptotic approaches agree well with that of the benchmark method, and in particular around the FS direction ($\theta_s = 180° - \theta_i = 155°$). Some differences between the classical PO and the PO combined with the BP can be observed from $\theta_s = 45°$ (and higher). Moreover, two discontinuities in the RCS computed from $\psi_{s,Ba+PO}(\mathbf{r}')$ can be

observed. The first one occurs at the frontier between Ω_1 and Ω_2 for $\theta_s = 45°$ (an enlarged detail is depicted in Fig. 9). Indeed, from this angle (and higher), $\psi_{s,1+}$ is set to zero in PO combined with BP. The second discontinuity occurs at the frontier between Ω_3 and Ω_4 for $\theta_s = 135°$ (an enlarged detail is depicted in Fig. 10), from which $\psi_{s,2+}$ is set to zero in PO combined with BP. Of course, these discontinuities do not appear with the classical PO method.

Fig. 11 compares the RCS of $\psi_{s,PO}(\mathbf{r}')$ and the RCS of its two components: the reflected one $\psi_{s,+}(\mathbf{r}')$ and the FS one $\psi_{s,-}(\mathbf{r}')$.
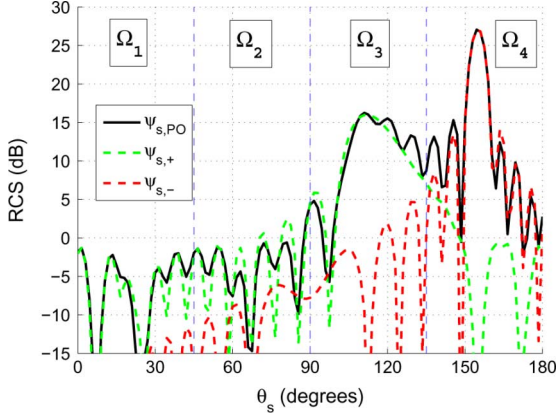
Fig. 11. Same simulation parameters as in Fig. 8, but computed from PO, PO in reflection, and PO in forward scattering.
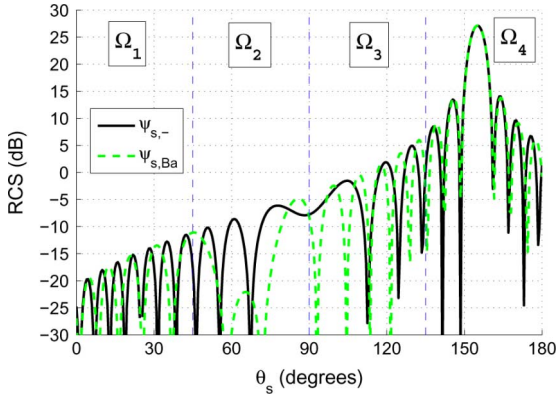

Fig. 12. Same simulation parameters as in Fig. 8, but computed from PO in forward scattering and BP.

Like for the first case, the reflected component decreases in the shadow region ($\psi_{s,+}(\boldsymbol{r}')$ being negligible in Ω_4), and the FS component becomes the main contribution to the scattered field.

Fig. 12 compares the RCS of the FS component, $\psi_{s,-}(\boldsymbol{r}')$, and the RCS of the BP, $\psi_{s,Ba}(\boldsymbol{r}')$.

Here, the two approaches do not match. Indeed, $B \neq 0$ and $z_m \neq 0$ since the two limit points of Σ_{PO} are not the same as those of the complementary Babinet screen Σ_{Ba} ($(x_{\min}^{PO}, z(x_{\min}^{PO})) \neq (x_{\min}^{Ba}, 0)$ and $(x_{\max}^{PO}, z(x_{\max}^{PO})) \neq (x_{\max}^{Ba}, 0)$) due to the equivalent rotation of the target. As already said, moving the emitter with a fixed target is equivalent to rotating the target with a fixed emitter. This third case is equivalent to that of a normal incidence (like for the first and second cases), but with a rotated triangularly shaped target with an angle $25°$. Thus, equalities (12) and (13) are only satisfied when $b_2 = 0$, implying $\theta_s = \pi - \theta_i$, which corresponds to the FS direction, for which $\boldsymbol{k}_i$ and $\boldsymbol{k}_s$ are collinear. As can be seen in Fig. 12, a perfect agreement is obtained in the FS direction $\theta_s = 155°$. The Babinet principle can be seen as an approximation of the PO approach, which provides exactly the same results as the PO in the FS direction. Moreover, it is shown in the Appendix that, for a scalar problem, the Cátedra currents exactly correspond to the classical PO approximation.

IV. CONCLUSION

For a 2-D problem, this paper shows that the BP can be derived from the PO approximation. Indeed, following the same idea as Ufimtsev, from the PO approximation and in far-field zone, the field scattered by an object can be split up into a field that mainly contributes around the specular direction (illuminated zone) and a field that mainly contributes around the forward direction (shadowed zone), which is strongly related to the scattered field obtained from the BP. The only difference relies on the integration surface.

A theoretical study has provided the mathematical proof that the involved integral in FS component of PO does not depend on the global shape of the object. Then, when the two limit points of Σ_{PO} are the same as those of the complementary Babinet screen Σ_{Ba}, then BP exactly corresponds to the FS component of PO. Thus, BP is included in the PO approximation. When the two limit points are not the same, BP can be seen as an approximation of the PO approach, and BP provides exactly the same results as PO in the FS direction. These theoretical conclusions were illustrated with the scattering from a triangularly shaped target to better investigate the link between BP and PO. In order to complete the study, the new PO approach, recently published by Cátedra *et al.* [9], was investigated for a scalar problem in the Appendix. This enables us to demonstrate that, for a scalar problem, the Cátedra currents exactly correspond to the classical PO approximation.

APPENDIX A
SCALAR CÁTEDRA APPROACH

In 2008, Cátedra *et al.* [9] proposed new induced PO currents to improve the FS computation. These currents extend over the whole body, including lit or shadowed parts. On the illuminated surface, the currents provide the reflected field ($\psi_{s,+}$), whereas on the shadowed surface, they provide the FS phenomenon ($\psi_{s,-}$). Applied to a scalar problem, for a perfectly conducting object, it can be shown that the Cátedra currents are given $\forall \boldsymbol{r} \in S$ in TE polarization by

$$\begin{cases} \psi(\boldsymbol{r}) = -\psi_i(\boldsymbol{r}) \\ \frac{\partial \psi(\boldsymbol{r})}{\partial n} = -\text{sign}(\boldsymbol{k}_i \cdot \hat{\boldsymbol{n}}) \frac{\partial \psi_i(\boldsymbol{r})}{\partial n} \end{cases} \tag{33}$$

and in TM polarization by

$$\begin{cases} \psi(\boldsymbol{r}) = -\text{sign}(\boldsymbol{k}_i \cdot \hat{\boldsymbol{n}})\psi_i(\boldsymbol{r}) \\ \frac{\partial \psi(\boldsymbol{r})}{\partial n} = -\frac{\partial \psi_i(\boldsymbol{r})}{\partial n}. \end{cases} \tag{34}$$

Since $\text{sign}(\boldsymbol{k}_i \cdot \hat{\boldsymbol{n}}) < 0$ on the illuminated surface Σ_{PO} of the target and $\text{sign}(\boldsymbol{k}_i \cdot \hat{\boldsymbol{n}}) \geq 0$ on the shadowed surface Σ_{Sh} ($S = \Sigma_{PO} \cup \Sigma_{Sh}$), (34) becomes

$$\begin{cases} \psi(\boldsymbol{r}) = +\psi_i(\boldsymbol{r}) & \forall \boldsymbol{r} \in \Sigma_{PO} \\ \psi(\boldsymbol{r}) = -\psi_i(\boldsymbol{r}) & \forall \boldsymbol{r} \in \Sigma_{Sh} \\ \frac{\partial \psi(\boldsymbol{r})}{\partial n} = -\frac{\partial \psi_i(\boldsymbol{r})}{\partial n} & \forall \boldsymbol{r} \in S. \end{cases} \tag{35}$$

Applying Huygens' principle (8) on these induced currents provides the scattered field in TM polarization and $\forall \boldsymbol{r}' \in \Omega$

$$
\psi_s(\boldsymbol{r}') = \int_{\Sigma_{\text{PO}}} \left[\psi_i(\boldsymbol{r}) \frac{\partial g(\boldsymbol{r}, \boldsymbol{r}')}{\partial n} + g(\boldsymbol{r}, \boldsymbol{r}') \frac{\partial \psi_i(\boldsymbol{r})}{\partial n} \right] d\Sigma
$$
$$
+ \int_{\Sigma_{\text{Sh}}} \left[-\psi_i(\boldsymbol{r}) \frac{\partial g(\boldsymbol{r}, \boldsymbol{r}')}{\partial n} + g(\boldsymbol{r}, \boldsymbol{r}') \frac{\partial \psi_i(\boldsymbol{r})}{\partial n} \right] d\Sigma. \tag{36}
$$

The second integral in the right-hand side corresponds to the scattering of the Babinet currents (10) applied on Σ_{Sh}. We have shown above that this integral does not depend on the surface contour, and by considering the normal $\hat{\boldsymbol{n}}$ oriented in the sense of positive $\hat{\boldsymbol{z}}$ for both integrals (change of sign in the second integral), (36) can be written as

$$
\psi_s(\boldsymbol{r}') = \int_{\Sigma_{\text{PO}}} \left[\psi_i(\boldsymbol{r}) \frac{\partial g(\boldsymbol{r}, \boldsymbol{r}')}{\partial n} + g(\boldsymbol{r}, \boldsymbol{r}') \frac{\partial \psi_i(\boldsymbol{r})}{\partial n} \right] d\Sigma
$$
$$
+ \int_{\Sigma_{\text{PO}}} \left[\psi_i(\boldsymbol{r}) \frac{\partial g(\boldsymbol{r}, \boldsymbol{r}')}{\partial n} - g(\boldsymbol{r}, \boldsymbol{r}') \frac{\partial \psi_i(\boldsymbol{r})}{\partial n} \right] d\Sigma
$$
$$
= \int_{\Sigma_{\text{PO}}} 2\psi_i(\boldsymbol{r}) \frac{\partial g(\boldsymbol{r}, \boldsymbol{r}')}{\partial n} \, d\Sigma \tag{37}
$$

which corresponds to the use of the classical PO approximation. Thus, for a scalar problem, the Cátedra currents provide exactly the same results as PO. The same conclusion can be drawn in TE polarization.

REFERENCES

[1] K. M. Siegel, "Bistatic radars and forward scattering," in *Proc. Aero Electron. Nat. Conf.*, Dayton, OH, 1958, pp. 286–290.

[2] J. I. Glaser, "Bistatic RCS of complex objects near forward scatter," *IEEE Trans. Aerosp. Electron. Syst.*, vol. AES-21, no. 1, pp. 70–78, Jan. 1985.

[3] J. I. Glaser, "Some results in the bistatic radar cross section (RCS) of complex targets," *Proc. IEEE*, vol. 77, no. 5, pp. 639–648, May 1989.

[4] P. S. Kildal, A. A. Kishk, and A. Tengs, "Reduction of forward scattering from cylindrical objects using hard surfaces," *IEEE Trans. Antennas Propag.*, vol. 44, no. 11, pp. 1509–1520, Nov. 1996.

[5] P. Y. Ufimtsev, *Fundamentals of the Physical Theory of Diffraction*. Hoboken, NJ: Wiley, 2007.

[6] P. Y. Ufimtsev, "Blackbodies and shadow radiation," *Sov. J. Commun., Technol. Electron.*, vol. 35, no. 5, pp. 108–116, 1990.

[7] P. Y. Ufimtsev, "Blackbodies and the problem of invisible objects," in *Proc. JINA*, 1992.

[8] P. Y. Ufimtsev, "New insight into the classical Macdonald physical optics approximation," *IEEE Antennas Propag. Mag.*, vol. 50, no. 3, pp. 11–20, Jun. 2008.

[9] M. F. Cátedra, C. Delgado, and I. G. Diego, "New physical optics approach for an efficient treatment of multiple bounces in curved bodies defined by an impedance boundary condition," *IEEE Trans. Antennas Propag.*, vol. 56, no. 3, pp. 728–736, Mar. 2008.

[10] B. B. Bakker and E. T. Copson, *The Mathematical Theory of Huygens Principle*. Oxford, U.K.: Oxford Univ. Press, 1939.

[11] M. Born and E. Wolf, *Principles of Optics*. New York: Pergamon, 1959.

[12] H. G. Booker, "Slot aerials and their relation to complementary wire aerials (Babinet's principle)," *Proc. Inst. Elect. Eng.*, vol. 93, pp. 620–626, 1946.

[13] P. Poincelot, "Sur le théorème de Babinet au sens de la théorie électromagnétique," *Ann. Télécommun.*, vol. 12, no. 12, pp. 410–414, Dec. 1957.

[14] P. Pouliguen, J. F. Damiens, and R. Moulinet, "Radar signatures of helicopter rotors in great bistatism," in *Proc. APS/URSI*, Jun. 2003, pp. 536–539.

Gildas Kubické was born in Longjumeau, France, in 1982. He received the Engineering degree and M.S. degree in electronics and electrical engineering from Polytech'Nantes (Ecole polytechnique de l'université de Nantes), Nantes, France, in 2005, and the Ph.D. degree in electronics from the University of Nantes, Nantes, France, in 2008.

He is currently working in the field of radar signatures at the Direction Générale de l'Armement (DGA), DGA-Maîtrise de l'Information, Bruz, France. He is also in charge of the Expertise and electoMagnetism Computation (EMC) Laboratory of DGA-Maîtrise de l'Information. His research interests include electromagnetic scattering and radar cross-section modeling.

Yacine Ait Yahia, photograph and biography not available at the time of publication.

Christophe Bourlier (M'99) was born in La Flèche, France, in 1971. He received the M.S. degree in electronics from the University of Rennes, Rennes, France, in 1995, and the Ph.D. degree in electronics from the Polytech'Nantes (University of Nantes, Nantes, France), in 1999.

While at the University of Rennes, he was with the Laboratory of Radiocommunication, where he worked on antennas coupling in the VHF-HF band. Currently, he is with the Institut de Recherche en Electrotechnique et Electronique de Nantes Atlantique (IREENA) Laboratory in the SEC team at Polytech'Nantes. He works as an Assistant Researcher with the National Center for Scientific Research on electromagnetic wave scattering from rough surfaces and objects for remote sensing applications. He is the author of more than 120 journal articles and conference papers.

Nicolas Pinel (A'09) was born in Saint-Brieuc, France, in 1980. He received the Engineering degree and M.S. degree in electronics and electrical engineering from Polytech'Nantes (Ecole polytechnique de l'université de Nantes), Nantes, France, in 2003, and the Ph.D. degree in electronics from the University of Nantes, Nantes, France, in 2006.

He is currently a Research Engineer with the Institut de Recherche en Électrotechnique et Électronique de Nantes Atlantique (IREENA) Laboratory, Nantes, France. His research interests are in the areas of radar, optical remote sensing, and propagation. In particular, he works on asymptotic methods of electromagnetic wave scattering from rough surfaces and layers.

Philippe Pouliguen was born in Rennes, France, in 1963. He received the M.S. degree in signal processing and telecommunications and the Ph.D. degree in electronics from the University of Rennes 1, Rennes, France, in 1986 and 1990, respectively.

In 1990, he joined the Direction Générale de l'Armement (DGA) at the Centre d'Electronique de l'Armement (CELAR), Bruz, France, where he was a DGA expert in electromagnetic radiation and radar signatures analysis. He was also in charge of the Expertise and electoMagnetism Computation (EMC) laboratory of CELAR. Now, he is the Head of acoustic and radio-electric waves domain at the Office for Advanced Research and Innovation of the Strategy Directorate, DGA, France. His research interests include electromagnetic scattering and diffraction, radar cross section (RCS) measurement and modeling, asymptotic high frequency methods, radar signal processing and analysis, antenna scattering problems, and electronic band-gap materials. In these fields, he has published more than 28 articles in refereed journals and more than 80 conference papers.